

SUPERLATTICE INTERMEDIATE BAND SOLAR CELL ON GALLIUM ARSENIDE

Alexandre Freundlich

**University of Houston
4800 Calhoun
Houston, TX 77204**

9 Feb 2015

Final Report

APPROVED FOR PUBLIC RELEASE; DISTRIBUTION IS UNLIMITED.



**AIR FORCE RESEARCH LABORATORY
Space Vehicles Directorate
3550 Aberdeen Ave SE
AIR FORCE MATERIEL COMMAND
KIRTLAND AIR FORCE BASE, NM 87117-5776**

DTIC COPY NOTICE AND SIGNATURE PAGE

Using Government drawings, specifications, or other data included in this document for any purpose other than Government procurement does not in any way obligate the U.S. Government. The fact that the Government formulated or supplied the drawings, specifications, or other data does not license the holder or any other person or corporation; or convey any rights or permission to manufacture, use, or sell any patented invention that may relate to them.

This report is the result of contracted fundamental research deemed exempt from public affairs security and policy review in accordance with SAF/AQR memorandum dated 10 Dec 08 and AFRL/CA policy clarification memorandum dated 16 Jan 09. This report is available to the general public, including foreign nationals. Copies may be obtained from the Defense Technical Information Center (DTIC) (<http://www.dtic.mil>).

AFRL-RV-PS-TR-2015-0048 HAS BEEN REVIEWED AND IS APPROVED FOR
PUBLICATION IN ACCORDANCE WITH ASSIGNED DISTRIBUTION STATEMENT.

//SIGNED//
DAVID WILT
Program Manager

//SIGNED//
PAUL HAUSGEN
Technical Advisor, Spacecraft Component Technology Branch

//SIGNED//
JOHN BEAUCHEMIN
Chief Engineer, Spacecraft Technology Division
Space Vehicles Directorate

This report is published in the interest of scientific and technical information exchange, and its publication does not constitute the Government's approval or disapproval of its ideas or findings.

REPORT DOCUMENTATION PAGE			Form Approved OMB No. 0704-0188		
Public reporting burden for this collection of information is estimated to average 1 hour per response, including the time for reviewing instructions, searching existing data sources, gathering and maintaining the data needed, and completing and reviewing this collection of information. Send comments regarding this burden estimate or any other aspect of this collection of information, including suggestions for reducing this burden to Department of Defense, Washington Headquarters Services, Directorate for Information Operations and Reports (0704-0188), 1215 Jefferson Davis Highway, Suite 1204, Arlington, VA 22202-4302. Respondents should be aware that notwithstanding any other provision of law, no person shall be subject to any penalty for failing to comply with a collection of information if it does not display a currently valid OMB control number. PLEASE DO NOT RETURN YOUR FORM TO THE ABOVE ADDRESS.					
1. REPORT DATE (DD-MM-YYYY) 09-02-2015		2. REPORT TYPE Final Report		3. DATES COVERED (From - To) 16 Nov 2012 to 30 Sep 2014	
4. TITLE AND SUBTITLE Superlattice Intermediate Band Solar Cell on Gallium Arsenide			5a. CONTRACT NUMBER FA9453-13-1-0232		
			5b. GRANT NUMBER		
			5c. PROGRAM ELEMENT NUMBER 62601F		
6. AUTHOR(S) Alexandre Freundlich			5d. PROJECT NUMBER 8809		
			5e. TASK NUMBER PPM00016788		
			5f. WORK UNIT NUMBER EF120624		
7. PERFORMING ORGANIZATION NAME(S) AND ADDRESS(ES) University of Houston 4800 Calhoun Houston, TX 77204			8. PERFORMING ORGANIZATION REPORT NUMBER		
9. SPONSORING / MONITORING AGENCY NAME(S) AND ADDRESS(ES) Air Force Research Laboratory Space Vehicles Directorate 3550 Aberdeen Ave. S.E. Kirtland AFB, NM 87117-5776			10. SPONSOR/MONITOR'S ACRONYM(S) AFRL/RVSV		
			11. SPONSOR/MONITOR'S REPORT NUMBER(S) AFRL-RV-PS-TR-2015-0048		
12. DISTRIBUTION / AVAILABILITY STATEMENT Approved for public release; distribution is unlimited.					
13. SUPPLEMENTARY NOTES					
14. ABSTRACT The design and practical viability of an intermediate band solar cell incorporating low dimensional structures made with dilute nitrogen alloys of III-V semiconductors is investigated theoretically and experimentally. Modeling of optical and electronic properties of the proposed materials and device is undertaken. The study suggests potential for this new class of single junction devices to yield efficiencies and radiation tolerance comparable or exceeding those of existing multi-junction devices.					
15. SUBJECT TERMS grant/cooperative agreement, III-V semiconductor, solar cell, superlattice, hifg efficiency					
16. SECURITY CLASSIFICATION OF:			17. LIMITATION OF ABSTRACT	18. NUMBER OF PAGES	19a. NAME OF RESPONSIBLE PERSON
a. REPORT Unclassified	b. ABSTRACT Unclassified	c. THIS PAGE Unclassified	Unlimited	34	David Wilt
					19b. TELEPHONE NUMBER (include area code)

--- This Page Intentionally Left Blank ---

TABLE OF CONTENTS

List of Figures	ii
Acknowledgments.....	iii
1 Summary	1
2 Introduction.....	2
3 Methods, Assumptions, and Procedures	4
3.1 Material selection and modeling of the superlattice absorption properties.....	4
3.1.1 Material selection and band-structure calculations.....	4
3.1.2 Calculation of the absorption properties of the superlattices.....	5
3.2 Simulation of Device Performance.....	6
3.2.1 Detailed Balance Simulations	6
3.2.2 Drift-Diffusion simulations and modeling of radiation effects.....	7
4 Results and Discussion	8
4.1 Detailed balance simulation of the device accounting for SL absorption.....	8
4.2 Drift Diffusion Efficiency Simulations	9
4.2.1 Optimizing superlattice and emitter thicknesses.....	9
4.2.2 Optimizing the bandgaps of the superlattice and the AlGaAs host cell.....	10
4.2.3 Effect of Sunlight Concentration (terrestrial applications).....	11
4.2.4 Evaluation of Device End-of Life Efficiencies.....	12
4.3 Discussion on Effect of relative absorption strength for inter-sub-band transitions.....	14
5 Conclusions.....	16
6 Recommendations.....	17
References.....	18
APPENDIX: Methodology for Calculaton of Minband Energies and Absorption Coefficient of a Superlattice.....	19
List of Acronyms, Abbreviations, and Symbols	24

LIST OF FIGURES

Figure 1. Energy diagram (left) and schematic view (right) of the proposed device.	3
Figure 2. Calculated band structure for AlGaAs & GaAsN material system & example of composition selection Al and N.	4
Figure 3. Absorption coefficient extracted from spectroscopic ellipsometry measurements of a pseudomorphically strained bulk GaAsN grown on GaAs (100).	5
Figure 4. Calculated absorption coefficient of a 30 period $\text{GaAs}_{0.98}\text{N}_{0.02}$ (3nm)/ $\text{Al}_{0.20}\text{Ga}_{0.80}\text{As}$ (3nm) Superlattice following the methodology developed in	6
Figure 5. Detail balance theoretical efficiency of an IBSC device with inclusion of absorption properties of a 0.5 micron SL region.	8
Figure 6. Detailed Balance efficiency contour plots for 1000 sun illumination as a function of Superlattice energy (E_i) and bandgap of host cell material (E_g)	9
Figure 7. Drift Diffusion simulation of the proposed IBSC for a 1.8eV AlGaAs with 1.2 eV GaAsN/AlGaAs superlattice region.	10
Figure 8. (a) Evolution of AM0 Efficiency as a function of AlGaAs bandgap. (b) a contour plot with AlGaAs bandgap of 1.85eV and miniband energy at 1.2 eV.	11
Figure 9. Drift-Diffusion Simulation of the AM1.5 efficiency as function of concentration and SL region thickness.	12
Figure 10. Evolution of max AM0 end of life efficiency as a function of 1MeV equivalent radiation fluence doses.	13
Figure 11. (a) Contour plot of device EOL efficiency as a function of emitter and i-region thickness for a 1MeV electron fluence dose of $2 \times 10^{15} \text{cm}^{-2}$ (b) EOL I-V characteristic of the device.	14
Figure 12. Evolution of device efficiency as a function of the ratio of absorption coefficients for transitions from the SL-miniband to conduction band of AlGaAs and from valence band to SL-miniband.	15

ACKNOWLEDGMENTS

We would like to thank the many people, particularly David Wilt, at Kirtland, who have worked diligently to put together helpful technical-report guidance for both contractors and government staff. Generated over many years, this existing content was the basis of the current document.

This material is based on research sponsored by Air Force Research Laboratory under agreement number FA9453-13-1-0232. The U.S. Government is authorized to reproduce and distribute reprints for Governmental purposes notwithstanding any copyright notation thereon.

DISCLAIMER

The views and conclusions contained herein are those of the authors and should not be interpreted as necessarily representing the official policies or endorsements, either expressed or implied, of Air Force Research Laboratory or the U.S. Government.

This Page Intentionally Left Blank

1 SUMMARY

This work evaluates the viability of an intermediate band solar cell design, wherein a superlattice, comprising lattice-matched layers of electronically mismatched $\text{GaAs}_{1-x}(\text{Sb})\text{N}_x$ ($x < 0.04$) and thin barriers of $\text{Al}_x\text{Ga}_{1-x}\text{As}$ ($x < 0.3$), is inserted within the intrinsic region of a wide bandgap AlGaAs p-i-n diode. In the proposed design the upper conduction band of GaAsSbN is maintained in resonance with the barrier conduction band of host material to promote an efficient extraction of electrons, whereas the 3D nature of the this band favors a strong intermediate (superlattice fundamental miniband) - to band second photon absorption.

The influence of device design parameters upon efficiency are extracted using drift diffusion-based simulations, that incorporates calculation of the absorption properties of the superlattice (SL) region and the host AlGaAs p-i-n solar cell, along with realistic semiconductor parameters. It is shown that through a careful device design optimization practical 1 sun efficiencies exceeding 33% (AM0), 36% (AM1.5) may be achieved. Analyses of device performance, under concentrated sunlight, show the potential for 45% efficiency under 500 suns illumination. An investigation of the radiation tolerance of the proposed device suggests that End of Life efficiencies in excess of 29% AM0 are possible.

The study suggest that this new class of highly efficient and radiation resistant, single junction solar cells could deliver practical performance comparable or exceeding that of existing multi-junctions devices. Considering the device absorber thicknesses and reduced complexity in terms of current matching/lattice matching, the proposed device also offers a path for significant improvements in term of specific efficiencies, reliability and manufacturing costs.

2 INTRODUCTION

The intermediate band solar cell (IBSC) presents a somewhat simpler single-junction device alternative to multijunction devices, where the presence of an intermediate band between the conduction and valence bands allows electrons to be promoted either directly to the conduction band via a single high-energy photon, or via the intermediate band with two low-energy photons [1]. As only the population of two lower energy transitions (valence band to IB and IB to conduction band) have to satisfy equality, the current-matching constraint, by comparison to multijunction devices, is partially relaxed. The cell has the voltage of the highest energy bandgap, provided the bands are thermally isolated. The cell can also capture the solar energy from low-energy photons. The theoretical efficiency of an ideal IBSC device is predicted to approach 45% and 63% under 1 sun and maximum sunlight concentration, respectively [1]. Thus far efforts to produce IBSCs have mainly focused on quantum dot (or quantum well) technologies based on conventional compound semiconductors (i.e. InGaAs/GaAs material system) which have not yet shown substantial IBSC (2 photons) photo-generation [2-4]

Recently strong two photon absorption/IBSC behavior has been reported for highly electronically mismatched bulk alloys [5,6] like in dilute nitrogen alloys of GaAs (GaAsN). In such alloys the interaction between the highly localized impurity-like states of nitrogen with that of the conduction band of the host crystal leads to a splitting of the conduction band with an upper band denoted here E^+ and a lower branch denoted E^- . The E^- conduction band is responsible for the unusual band gap shrinkage observed for the dilute nitride alloys (~ 150 meV/percent of nitrogen) and the increase of electron effective masses that are at the origin of exceptionally strong near band-edge absorption properties of these alloys. Unfortunately the introduction of nitrogen in these alloys is often accompanied with severe shortening of minority carrier diffusion lengths commonly believed as the main cause for open circuit voltage degradations in dilute nitride devices.

Building on the encouraging results shown by Lopez and co-workers [5], here we evaluate a superlattice intermediate band solar cell, wherein a superlattice comprising lattice matched layers of electronically mismatched alloys and thin barriers are inserted within the intrinsic region of a wide bandgap p-i-n diode. In the proposed design (Figure 1) the upper conduction band of the mismatched alloys is maintained to be in resonance with the barrier and bandgap of host material to promote an efficient extraction of electrons, where the choice of shallow valence band offsets favors the minority hole extraction, and the intermediate level is built through superlattice minibands formed by coupling lower band gap (lower conduction branch of mismatched alloys) wells. Here carriers can be promoted either directly to the conduction band or via the intermediate band, permitting the absorption of low energy photons whilst maintaining a high cell voltage. Also the characteristic lengths of the wells can be chosen to be substantially smaller than typical diffusion lengths of the electronically mismatched alloy [7], an approach has been shown to overcome the minority carrier losses observed in bulk materials [8]. To attain the necessary combination of high and low bandgaps and low dislocation density, we use materials that are lattice-matched to a GaAs (or Ge) substrate.

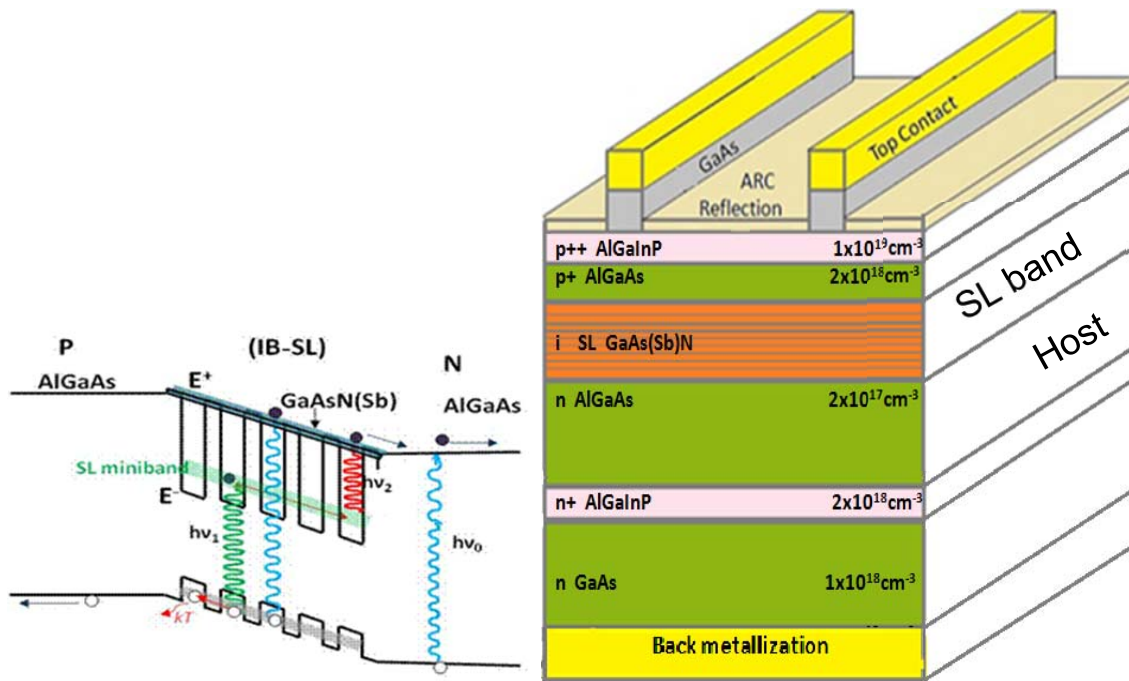


Figure 1. Energy diagram (left) and schematic view (right) of the proposed device.

Within the framework of this investigation we have undertaken a modeling of the superlattice absorption properties and accounted for these properties to derive both somewhat idealist detailed balance and practical drift-diffusion type efficiency analyses. The study also included gauging the potential radiation tolerance of the proposed design. The modeling effort was completed by also evaluating within the parameter design space best combination for maximum efficiency under 1 sun and concentrated sunlight conditions.

3 METHODS, ASSUMPTIONS, AND PROCEDURES

Method assumptions and procedures both for the modeling and experimental component of the work are summarized below.

3.1 Material selection and modeling of the superlattice absorption properties

The information that follows in Sections 3.1.1-3.1.3 provides useful information for the body of the technical report.

3.1.1 Material selection and band-structure calculations

To attain the necessary combination of high and low bandgaps and low dislocation density, we use materials that are lattice-matched to a GaAs (or Ge) substrate. In our design we contemplate GaAs_{1-x-y}N_xSb_y or GaAsN quantum well layers that are lattice matched to GaAs and will be incorporated into direct bandgap low Al content (x<30%) AlGaAs host material, to attain high bandgaps of 1.8- 1.9 eV, and low-energy bandgaps of 1-1.2 eV. In fact the anti-crossing interaction between the N-localized state and the conduction band of host III-V matrix. The new conduction sub-bands originated by such a splitting due to the N induced perturbation are denoted as E₋ and E₊ and are given as [9],

$$E_{\pm}(k) = \frac{1}{2} \left\{ E_N + E_{III-V}(k) \pm \sqrt{(E_N - E_{III-V}(k))^2 + 4xV_N^2} \right\} \quad (1)$$

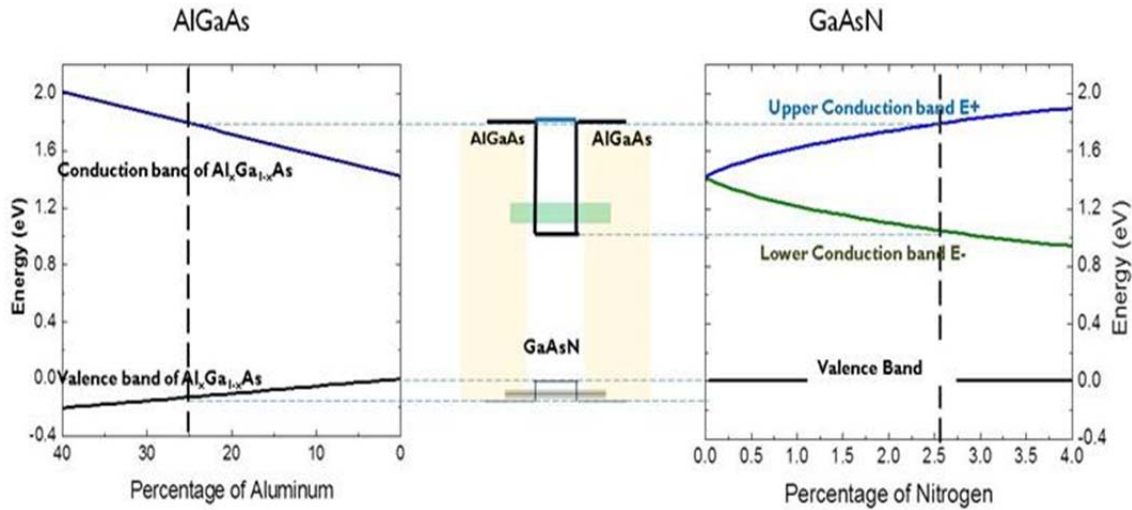


Figure 2. Calculated band structure for AlGaAs & GaAsN material system & example of composition selection Al and N.

where E_N is the energy of the localized nitrogen state, $E_{III-V}(k)$ is the dispersion of the host crystal conduction band, V_N is the strength of the anti-crossing interaction between the nitrogen localized states and the conduction band states of host matrix, and x is the nitrogen

concentration. All the energies are relative to the valence band maximum of the unperturbed host crystal. The band anticrossing in GaInNAs Alloys (BAC) model with $V_N=2.7\text{eV}$ provides an excellent fit for the nitrogen concentration $x\sim 0.04$. The E- and E+ conduction band branches of the dilute nitride alloy have an energy separation that is generally set by the nitrogen composition of the dilute nitride material. The calculated band structure for AlGaAs and GaAsN material system is shown in Figure 2. The shaded minibands in Figure 2 correspond to fundamental electron (green) and heavy hole (gray) bands in 3 nm GaAsN (N \sim 2.5%).

The use of thin barriers and wells can be used to adjust the miniband energies hence providing an additional degree of freedom in the energy of the intermediate band energy independently from the E+ energy level. Here the shallow valence band offsets favor a rapid thermionic escape of holes at a time scale of a few picoseconds. Note considering the deep electron wells the thermo-ionic escape of electrons from the intermediate level exceeds the nanosecond scale and hence the only possible escape route is the absorption of the second photon.

3.1.2 Calculation of the absorption properties of the superlattices.

The calculation of the SL region absorption properties follow a previously established methodology [10, 11]. The methodology includes the extraction of the superlattice miniband energies using the transfer matrix method and a formalism detailed in Appendix A is then applied to extract the absorption coefficient. The formalism associated with calculation of miniband energies and the absorption coefficient is detailed in Appendix A.

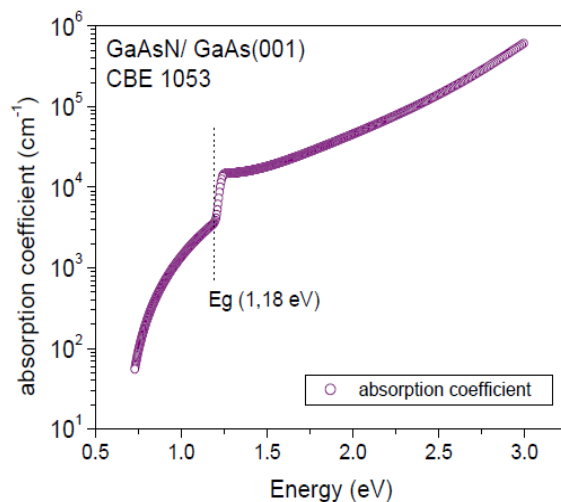


Figure 3. Absorption coefficient extracted from spectroscopic ellipsometry measurements of a pseudomorphically strained bulk GaAsN grown on GaAs (100).

The simulation effort included modification of the existing Matlab-based custom source code for superlattice to include material parameters for dilute nitride and AlGaAs alloys. The calculation account for strain Hamiltonian and band-anti-crossing effects. Absorption of the bulk dilute

nitride was extracted from spectroscopic ellipsometry measurements of previously grown bulk pseudomorphically strained layers of 1.2 eV GaAsN shown in Figure 3.

An example of the calculation of the absorption properties of the intermediate band superlattice structure incorporating 30 period of a 5nm thick GaAsN wells and 5nm thick AlGaAs barriers is shown in Figure 4.

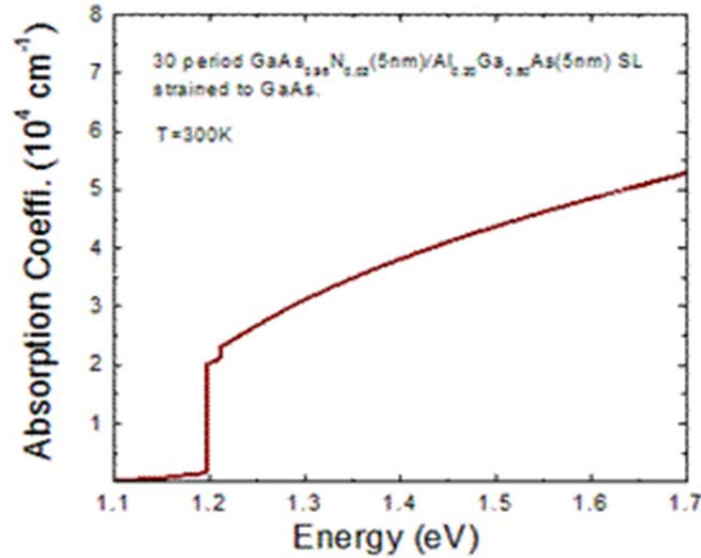


Figure 4. Calculated absorption coefficient of a 30 period GaAs_{0.98}N_{0.02} (3nm)/ Al_{0.20}Ga_{0.80}As (3nm) Superlattice following the methodology developed in ref 10.

3.2 Simulation of Device Performance.

This portion of the modeling effort relied on simulations of the device I-V characteristics and efficiencies using a Detailed-Balance (thermodynamic somewhat idealist model) and Drift Diffusion based approach. Existing Matlab-based custom codes were modified to incorporate the chosen parameters and assumption detailed hereafter in the code

3.2.1 Detailed Balance Simulations

The detailed balance modeling approach was similar to the one described in reference 1, except that to add a higher degree of realism the modeling accounted for the absorption properties and finite thicknesses of SL intermediate band (IB) region. To simulate the efficiencies we have extrapolated absorption properties calculated in Figure 4. These calculations were performed both under space sunlight illumination (AM0) and terrestrial (AM1.5G) conditions.

3.2.2 Drift-Diffusion simulations and modeling of radiation effects

In order to gain a more realistic insight on the potential of the proposed design we have undertaken a drift-diffusion modeling as a function emitter and base thicknesses and doping and by incorporating realistic minority carrier lifetimes and Shockley Reed Hall (SRH) recombinations using a previously established methodology [12]. For the superlattice region we have assumed a superlattice comprising N period (N varied from 10-100) of 5nm AlGaAs barriers and 5nm GaAsN(Sb) wells. The simulations were carried out with AlGaAs n-type base doping range of 10^{17} to 10^{18}cm^{-3} while the p-type emitter doping range is between 10^{18} and $5 \times 10^{18}\text{cm}^{-3}$. SRH lifetime for depleted region is between 10^{-8} sec to 5×10^{-8} sec while the surface recombination velocity is in the order of 10^3cm/sec . For uniformity in results it is assumed 3% anti-reflective coating and 5% grid shadowing losses have been included. Minority carrier lifetimes as a function of doping concentration for GaAs instead of AlGaAs are taken including Shockley-Read-Hall effect, band to band recombination and Auger recombination. Minority carrier diffusion lengths and diffusion coefficient as a function of doping concentrations and absorption coefficient of material are taken from the experimental values in the literature.

Here we also attempted to simulate the effect of space radiation induced degradations by assuming a radiation induced degradation of minority carrier diffusion length similar to that of GaAs. The reduction in minority carrier diffusion length can be modeled according to relation,

$$L^{-2} = L_0^{-2} + K_L \phi \quad (2)$$

Where L is the net diffusion length, L_0 is the diffusion length of defect free III-V material, ϕ is the electron radiation fluence per cm^2 and K_L is radiation constant, which depends on the material used in the sub-cell. The K_L is taken equal to 3×10^{-8} for fluencies of 1 MeV electrons. It should be noted that analyses presented here do not account for carrier removal effects which in turn can affect the E-field across the superlattice region.

4 RESULTS AND DISCUSSION

4.1 Detailed balance simulation of the device accounting for SL absorption

To assess the photovoltaic potential of the proposed design we have undertaken a detailed balance modeling by assuming a device incorporating a 0.5 microns superlattice region with the intermediate band region absorption properties comparable to the one calculated in Fig 3. The preliminary calculation presented here assumes that all photons with energy larger than the bandgap of AlGaAs (or E⁺) are absorbed in the emitter of the device (thick emitter approximation) whereas photons with energy comprised between the fundamental miniband state and resonant E⁺ level are absorbed with absorption properties similar to that of the dilute nitride superlattice. The absorption strength for inter-subband photon absorptions between the fundamental and excited states of the superlattice has not been considered to account for the fact that under normal light incidence the transition from fundamental to first excited miniband state is forbidden and the oscillator strength for such transition in a pure 2D state is zero. Since here the inter-subband absorption between the fundamental or excited states (intermediate 2D band) to the upper conduction band and involves 3D like E⁺ states of the dilute nitride material/AlGaAs, thus the oscillator strength =0 selection rule does not limit the absorption as is the case for conventional superlattices. For the calculations presented here we have assumed, that within the limit of available photons for each photon absorbed by the IB a second photon is absorbed between IB and E⁺.

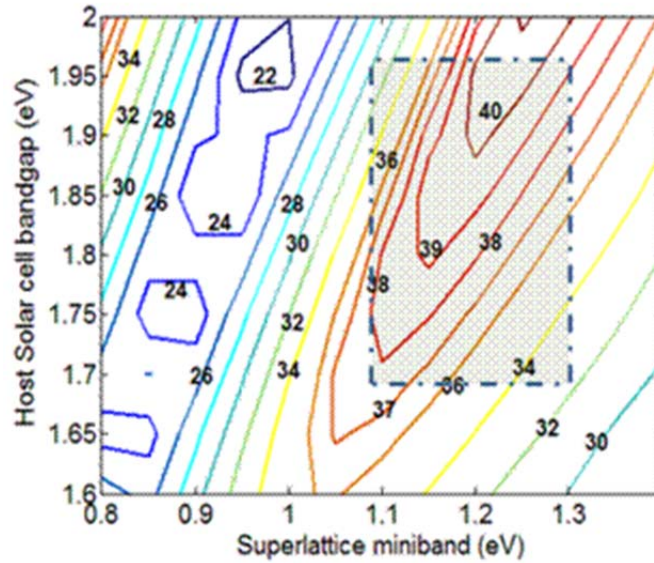


Figure 5. Detail balance theoretical efficiency of an IBSC device with inclusion of absorption properties of a 0.5 micron SL region.

The AM0 efficiency contour plots as a function of the superlattice fundamental miniband energy and the host bandgap for a superlattice IBSC device proposed here are shown in figure 5

(calculation accounts for 10% reflection and grid shadowing losses). The dotted rectangle in Figure 5 is for eye guidance and indicates the practical design space available with the proposed AlGaAs/GaAsSbN SL material system described in section 3-1.1. These somewhat idealist calculations stress the potential of the proposed IBSC for achieving 1sun-AM0 efficiencies in excess of 39%.

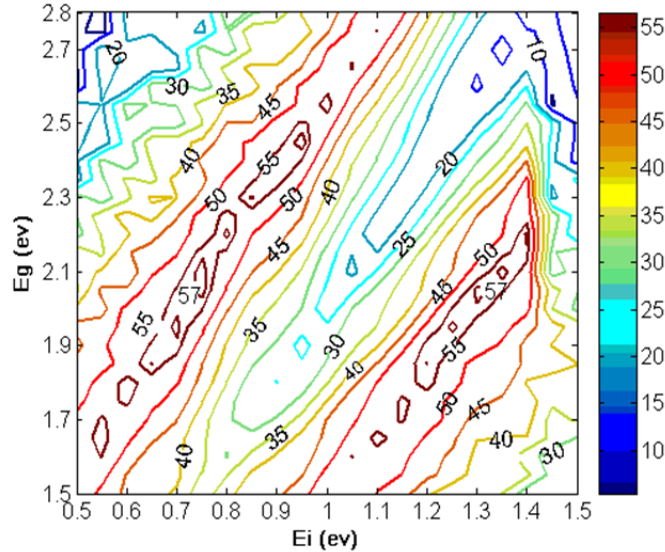


Figure 6. Detailed Balance efficiency contour plots for 1000 sun illumination as a function of Superlattice energy (E_i) and bandgap of host cell material (E_g)

Next we have extended the efficiency calculations under concentrated sunlight. In Figure 6 the efficiency contour plots for the proposed IBSC device are computed assuming a 0.5 micron thick superlattice region. This detailed balance simulation suggest sets an upper theoretical limit exceeding 55% for a device operating under 1000 sun AM1.5 illumination.

4.2 Drift Diffusion Efficiency Simulations

In order to gain a more realistic assessment of the potential of the proposed design we have undertaken the development of a drift-diffusion model as a function of emitter, base thickness, doping, and incorporating realistic minority carrier lifetimes and SRH .

4.2.1 Optimizing superlattice and emitter thicknesses

For the superlattice region we have assumed a superlattice comprising N period (N varied from 10-200) of 5nm AlGaAs barriers and 5nm GaAsNSb wells. Figure 7 shows the evolution of the AM0 efficiencies as a function of the i-region thickness and emitter thickness with a fixed base

thickness of 0.5 microns. For a 1.8 eV AlGaAs an 80-90 period SL with an emitter thickness of 0.5micron provides the highest AM0 efficiency of 31.4%.

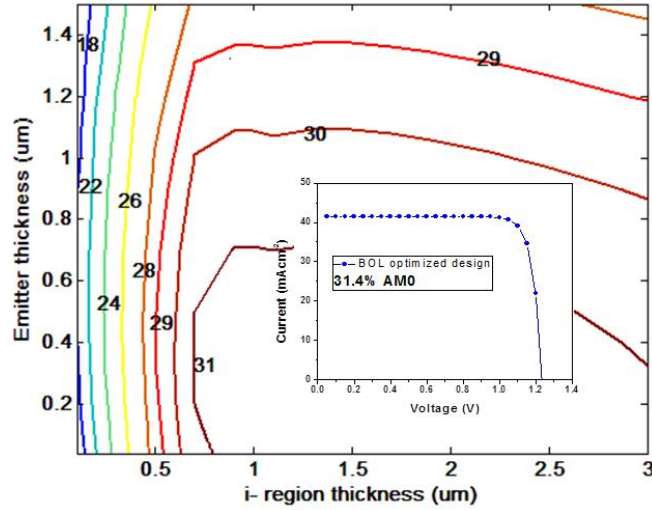


Figure 7. Drift Diffusion simulation of the proposed IBSC for a 1.8eV AlGaAs with 1.2 eV GaAsN/AlGaAs superlattice region.

It should be noted that due to strong below AlGaAs bandgap absorption in the superlattice region, in the device simulation for superlattice exceeding a thickness of 0.2 microns the device IV characteristics were found to be insensitive to the device base thickness. The IV characteristics for the best device in these conditions are shown in an inset in Figure 7.

4.2.2 Optimizing the bandgaps of the superlattice and the AlGaAs host cell

Next we have evaluated the effect of the miniband energy and the bandgap of host cell upon the evolution of device efficiency. A set of contour plots were generated as a function of the bandgap of the superlattice and the AlGaAs host bandgap. For the superlattice region individual layer thicknesses were adjusted to yield the targeted miniband energies of 1.1, 1.2 and 1.3 eV. Figure 8 represents the results of these calculations. Each data point in the Figure corresponds to the maximum efficiency extracted from full contour plot calculation similar to those shown in Fig 7.

Interestingly it is found that the AM0 efficiency can be further boosted by using a 1.9 eV AlGaAs material, with a targeted efficiency of ~34% AM0 (Figure 8a). It should be noted that from a practical standpoint it may be preferable to target a slightly lower host bandgap i.e. 1.85 eV which could yield an efficiency of ~33% (Figure 8b).

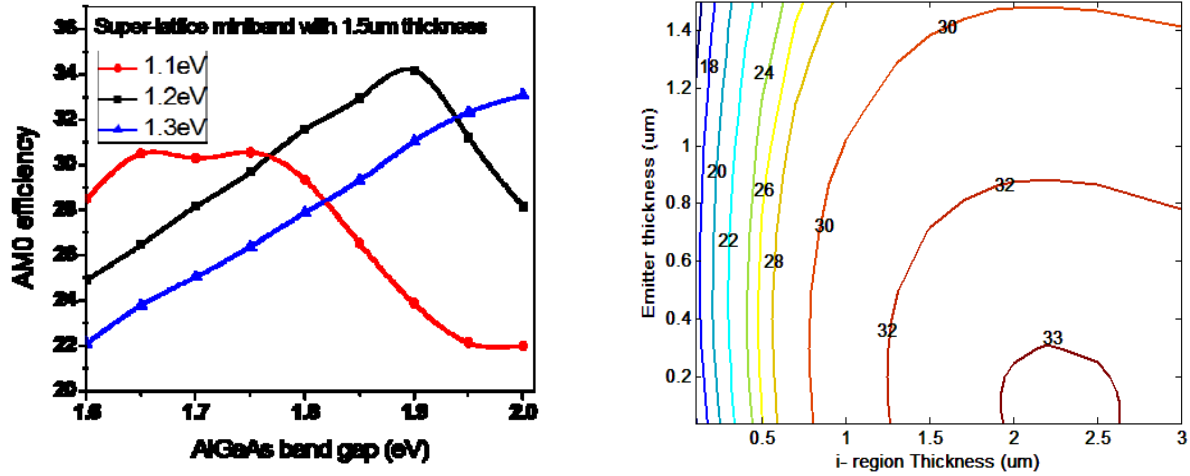


Figure 8. (a) Evolution of AM0 Efficiency as a function of AlGaAs bandgap. (b) a contour plot with AlGaAs bandgap of 1.85eV and miniband energy at 1.2 eV.

4.2.3 Effect of Sunlight Concentration (terrestrial applications)

We have also evaluated the potential of the technology for terrestrial and concentrator applications. Figure 9 shows the best efficiency recorded for AM1.5G illumination. A 1 sun efficiency of ~36% seems achievable by using a 1.2 eV superlattice and 1.85 eV AlGaAs. In Figure 9, each period of the superlattice is 10nm (i.e. 0.1microns= 10 periods).

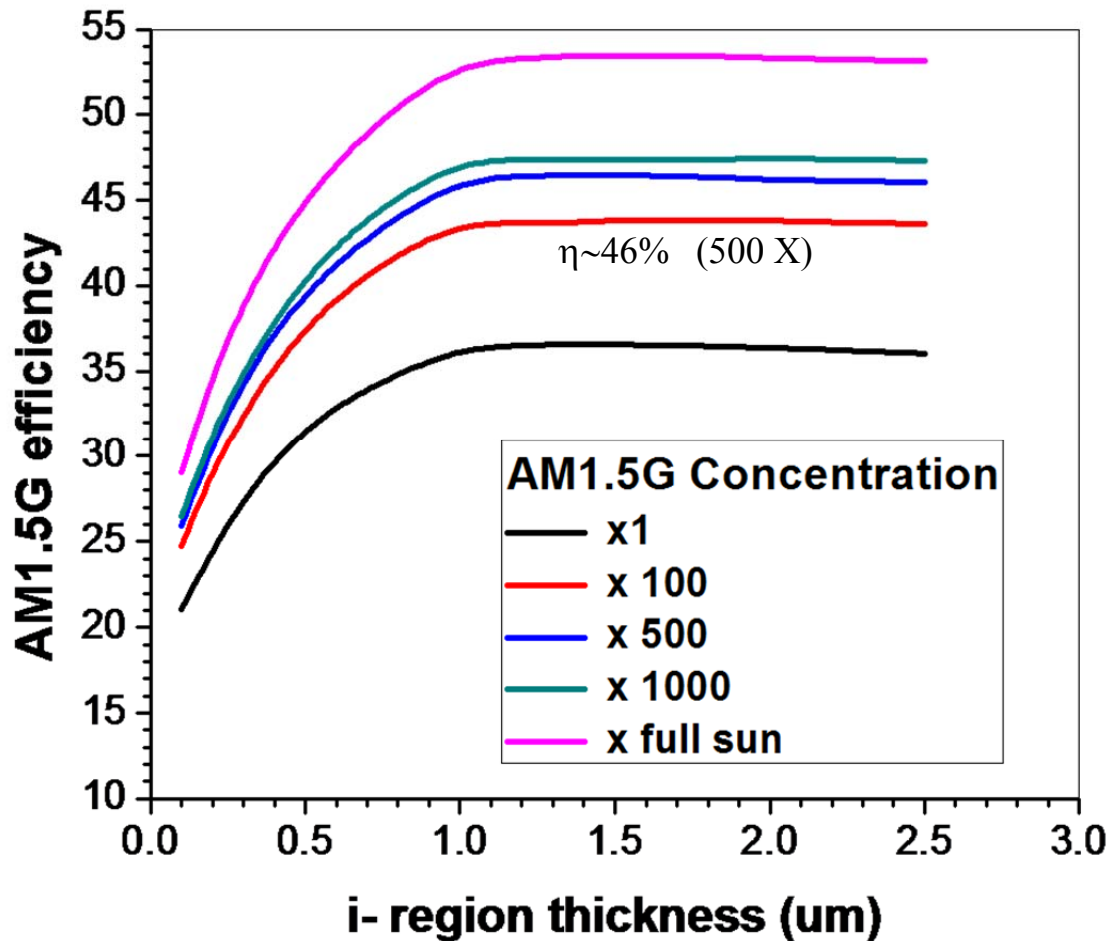


Figure 9. Drift-Diffusion Simulation of the AM1.5 efficiency as function of concentration and SL region thickness.

It is worth noting that these max efficiencies are reached for i-region thickness of ~ 2 microns (100 periods) assuming a fully depleted i-region which assumes a background carrier concentration/unintentional doping in the I region lower or about $\sim 10^{15} \text{cm}^{-3}$.

4.2.4 Evaluation of Device End-of Life Efficiencies

We next expanded our simulations to include the effect of radiation degradation to assess the end of life (EOL) efficiencies of these devices in space. Figure 10 represents the evolution of maximum achievable efficiency for variation radiation fluencies. Each calculation point is the outcome of the optimization of all design parameters. The dotted line in Figure 10 indicates the data point extracted from the contour plot and corresponding IV shown in Figure 11.

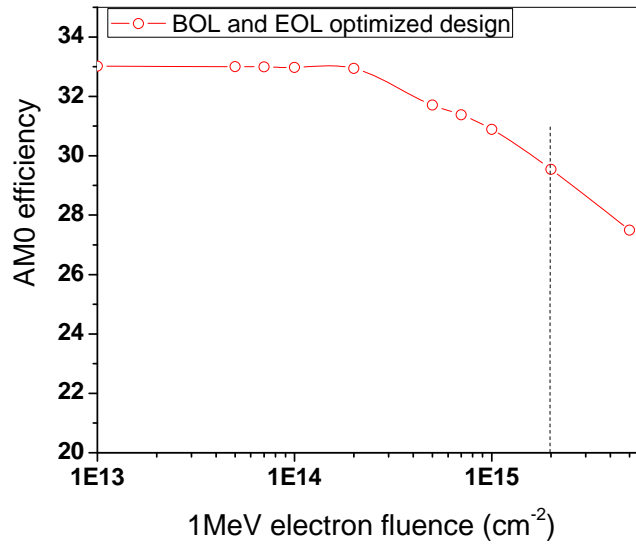


Figure 10. Evolution of max AM0 end of life efficiency as a function of 1MeV equivalent radiation fluence doses.

As an example for a radiation dose of $2 \times 10^{15} \text{ cm}^{-2}$, that corresponds to a degradation similar to 10 years operation in a geostationary orbit, a contour plot as a function of emitter and superlattice region for 1.2 eV superlattice/1.8eV AlGaAs, is shown in Figure 11. For the latest radiation dose the study indicates the potential to exceed EOL efficiencies of 29% AM0. It should be noted that the calculations do not account for carrier removal effects which could lead to a radiation induced increase of background carrier concentrations in the i-region which in turn may affect the carrier extraction processes from the i-region (E-field)

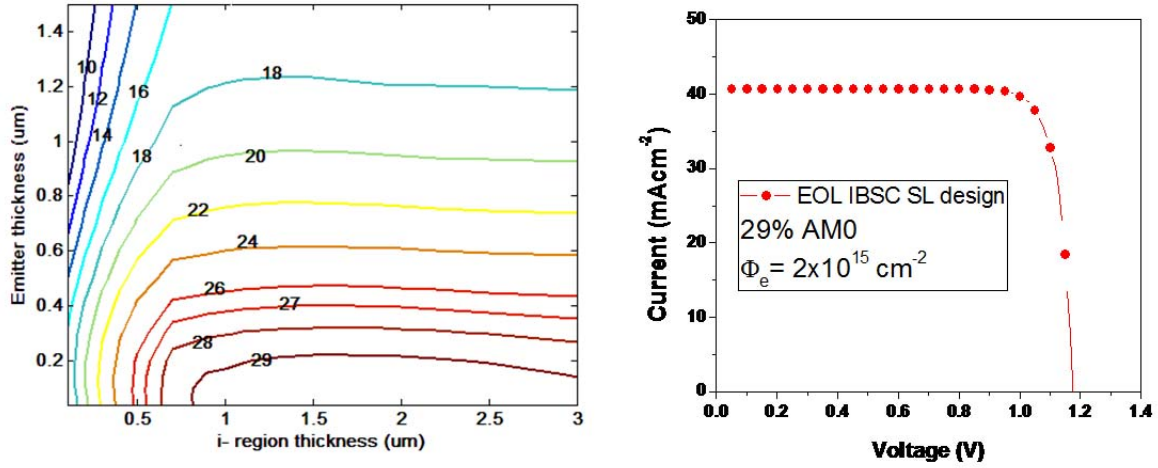


Figure 11. (a) Contour plot of device EOL efficiency as a function of emitter and i-region thickness for a 1MeV electron fluence dose of $2 \times 10^{15} \text{ cm}^{-2}$ (b) EOL I-V characteristic of the device.

4.3 Discussion on Effect of relative absorption strength for inter-sub-band transitions

The basic operation of an IBSC solar cell requires a strong absorption from the valence band to the intermediate band IB, a condition satisfied by the superlattice structure (Fig. 4), followed by an equally strong absorption/photo-promotion of carriers (here electrons, as hole band offset is negligible) from the superlattice fundamental miniband to the host cell continuum. In practical realization involving quantum dots or conventional Kane-like 2D superlattices and quantum wells this second absorption has been extremely weak [2-4]. The design contemplated in this work builds on a transition between the 1st miniband (E- band like behavior) and the continuum that is resonant with 3D like E+ states populated, and hence as shown for bulk like dilute nitrides, the 2nd photon induced electron promotions are stronger [5]. Yet it is important to gauge the actual strength of such inter-subband carrier promotion, as it requires both for the band to be populated and for the associated absorption coefficient to be strong. In the calculations presented in section 4.2 we have assumed that the absorption strength was similar to that of the miniband which may be a reasonable assumption as E- and E+ states have somewhat similar density of states, yet the overlap of wave functions (oscillator Strength) for the transition from E- or SL miniband to the upper conduction band E+ could be much weaker than that of the inter-band one (valence band (VB)-to -superlattice miniband). In the absence of actual measures for intersubband absorption coefficients in Figure 12 we represent the effect of the absorption coefficient mismatch between the two transitions on the device efficiency. It should be noted that while a small mismatch (i.e. factor of 2) has almost no effect on the maximum projected efficiency, for higher absorption mismatches the efficiency steeply decreases, to eventually drop below that of a single junction 1.8 eV solar cells (~20% AM0).

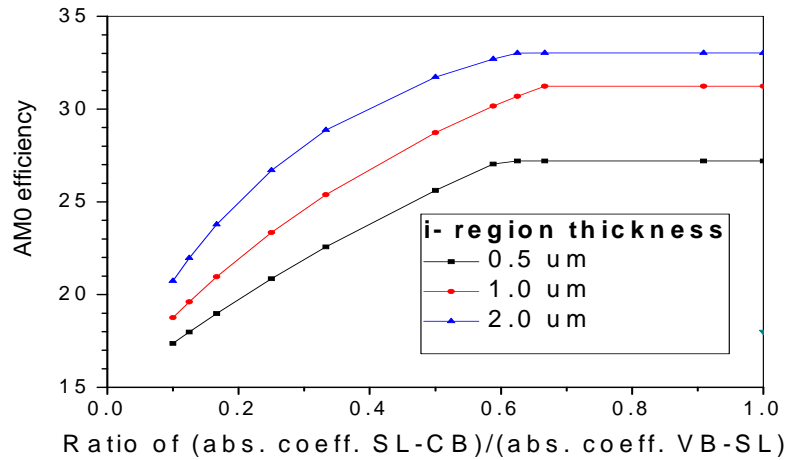


Figure 12. Evolution of device efficiency as a function of the ratio of absorption coefficients for transitions from the SL-miniband to conduction band of AlGaAs and from valence band to SL-miniband.

The calculation however assumes a single-pass normal light-path through the device and thus simply incorporating a reflective mirror at the back of the device should improve the 2 photon absorption/up-conversion processes. Ultimately, incorporation of a *Lambertian* reflector which could enhance the effective light path by $4n^2$ (n index of refraction ~ 3.4), i.e. 40 fold could be used to mitigate/or completely overcome the risk associated with weak inter-sub-band absorption for these devices.

5 CONCLUSIONS

In this work we investigated the potential for space and terrestrial applications of a novel single junction solar cell where a superlattice comprising well of 1-1.3 eV dilute nitride alloys and (1.7-1.9eV) AlGaAs barriers is inserted in the intrinsic (i) region of an AlGaAs p-i-n diode. The work included the simulation of band-structure and absorption properties of the superlattice. The latest were incorporated in a Detailed Balance and Drift-Diffusion simulator to extract somewhat ideal and practical efficiency limits of the device. The study included exploring a wide range of design parameters

The analyses indicated the potential for this single junction device to deliver efficiencies in excess of 33% under space sunlight illumination (AM0) and 46% under 1000 sun concentration. The effects of radiation-induced degradations were also incorporated. The potential for the device to deliver end-of-life efficiencies in excess of 29%AM0 for a radiation fluence of 10^{15}cm^{-2} 1MeV electron was predicted.

It should be noted that the technology provides a path to achieve efficiencies comparable to 4 junction device in several fold thinner single junction. The design also relieves to some extent the current-matching constrains of multijunction devices. Consequently by comparison to current state-of-the-art, the technology has the potential of enhancing both specific efficiencies and reliability of high efficiency space solar cells.

6 RECOMMENDATIONS

The device design studied here appears as promising however a key parameter toward the success of the approach is to the absorption strength of the intersubband transition from the superlattice miniband to the continuum. In our preliminary modeling we have shown the criticality of the interband absorption toward exceeding the efficiency limit of single junction devices. One approach to further strengthen the inter-subband absorption could consist of enhancing the optical path of light by incorporating a back reflector (i.e. gold) that recycles the transparency losses into the superlattice region. It should be noted that incorporation of a *Lambertian* reflector could potentially result in a $4 n^2$ enhancement of the effective absorption path. For III-V compounds contemplated here (index of refraction $n \sim 3.4$) this could present a 40 fold enhancement of the absorption strength. Development of such a reflector will also allow the device superlattice region to be made much thinner and hence in principle will improve the device radiation tolerance/end of life efficiencies.

REFERENCES

- [1] A. Luque and A. Martí, "Increasing the Efficiency of Ideal Solar Cells by Photon Induced Transitions at Intermediate Levels," *Phys. Rev. Lett.* **78** (1997) pp. 5014-5017.
- [2] Y. Okada, et al., "Increase in photocurrent by optical transitions via intermediate quantum states in direct-doped InAs/GaNAs strain-compensated quantum dot solar cell," *J. Appl. Phys.* **109** (2011) 024301.
- [3] A. Martí, et al., "Production of Photocurrent due to intermediate to-Conduction-Band Transitions: A Demonstration of a Key Operating Principle of the IBSC," *Phys. Rev. Lett.* **97** (2006) 247701.
- [4] M. Sugiyama, et al., "Photocurrent generation by two-step photon absorption with quantum well superlattice cell," Proceedings of the *37th IEEE Photovoltaic Specialists' Conference*, Seattle, WA (2011).
- [5] N. López, et al., "Engineering the Electronic Band Structure for Multiband Solar Cells," *Phys. Rev. Lett.* **106** (2011) 028701.
- [6] T. Tanaka, et al., "Demonstration of ZnTe_{1-x}O_x Intermediate Band Solar Cell," *Jpn. J. Appl. Phys.* **50** (2011) 082304.
- [7] A. Freundlich, et al., "III-V dilute nitride-based multi-quantum well solar cell," *Journal of Crystal Growth* **301-302** (2007) pp. 993-996.
- [8] A. Khan, et al., "Correlation of nitrogen related traps in InGaAsN with solar cell properties," *Appl. Phys. Lett.* **90** (2008) 243509.
- [9] W. Shan, et al., "Band Anticrossing in GaInNAs Alloys," *Phys. Rev. Lett.* **82** (1999) p. 1221.
- [10] L. Bhusal and A. Freundlich, "Band structure and absorption properties of GaAs_{1-x}N_x/InAs_{1-y}N_y short period superlattices strained to InP (001)," *Phys. Rev. B* **75** (2007) 075321.
- [11] A. Freundlich, G.K. Vijaya, and A. Mehrotra, "Superlattice Intermediate Band Solar Cell with Resonant Upper-Conduction-Band Assisted Photo-Absorption and Carrier Extraction," Proc. *39th IEEE PVSC*, Tampa, FL (2012).
- [12] A. Mehrotra, A. Alemu, and A. Freundlich, "Modeling and optimal design for dislocation and radiation tolerant single and multijunction devices," *Proc. SPIE* **7933** (2011) 79332G.

APPENDIX: METHODOLOGY FOR CALCULATION OF MINBAND ENERGIES AND ABSORPTION COEFFICIENT OF A SUPERLATTICE

A.1 Miniband Energy Calculation

For a fixed energy and fixed in-plane wave vectors k_x and k_y , we can construct the total envelope function of a superlattice as a linear combination of the eigenvectors of the corresponding Hamiltonian. For each region j , the full envelope function has the general shape

$$\Psi(z) = \sum_q a_q^j \mathbf{F}_q^j e^{ik_q^j(z-l_j)} + \sum_q b_q^j \mathbf{F}_q^j e^{-ik_q^j(z-l_j)} \quad (\text{A1})$$

where the sum is over all the bands q , conduction band and valence band, a_q^j and b_q^j are complex constants, \mathbf{F}_q^j are eigenvector matrices and l_j defines the j^{th} interface from the origin.

Boundary conditions at each interface are³⁹

$$\Psi^j \Big|_{z=l_j} = \Psi^{j+1} \Big|_{z=l_{j+1}} \quad \text{and} \quad \frac{1}{m_j} \frac{\partial \Psi^j}{\partial z} \Big|_{z=l_j} = \frac{1}{m_{j+1}} \frac{\partial \Psi^{j+1}}{\partial z} \Big|_{z=l_{j+1}} \quad (\text{A2})$$

Here, m_j is the effective mass in j^{th} layer. For $k_x=k_y=0$, the $m_j=\pm 3/2$ hole band gets decoupled from the rest of the bands, and transfer matrix can be found applying above two boundary conditions to relate constants a and b of the j^{th} and $(j+1)^{\text{th}}$ layers, and is given as

$$\begin{pmatrix} a^j \\ b^j \end{pmatrix} = M_{j(j+1)} \begin{pmatrix} a^{j+1} \\ b^{j+1} \end{pmatrix} \quad (\text{A3})$$

where

$$M_{j(j+1)} = \begin{pmatrix} 1 + \frac{m_j k_{j+1}}{m_{j+1} k_j} & 1 - \frac{m_j k_{j+1}}{m_{j+1} k_j} \\ 1 - \frac{m_j k_{j+1}}{m_{j+1} k_j} & 1 + \frac{m_j k_{j+1}}{m_{j+1} k_j} \end{pmatrix} \begin{bmatrix} e^{-ik_{j+1} L_{j+1}} & 0 \\ 0 & e^{ik_{j+1} L_{j+1}} \end{bmatrix} \quad (\text{A4})$$

Here, L_j is the thickness of the j^{th} layer. For large number of layers, the total transfer matrix can be written as the product of transfer matrices across each layer

$$\begin{pmatrix} a^1 \\ b^1 \end{pmatrix} = M_{total} \begin{pmatrix} a^N \\ b^N \end{pmatrix} \quad (A5)$$

$$M_{total} = \begin{pmatrix} m_{11} & m_{12} \\ m_{21} & m_{22} \end{pmatrix} = M_{12} M_{23} M_{34} \dots$$

We now require $a^1 = b^N = 0$ for decaying solutions in the first and last barriers, width of which is assumed to be large enough for this condition to hold. To satisfy this condition, the element m_{11} goes to zero and hence the solution of equation $m_{11}(E)=0$ provides the energy states of the corresponding carriers in $m_j=\pm 3/2$ hole states. Same process can be repeated for $m_j=\pm 1/2$ states also, but due to the interaction with spin orbit split-off states we have to deal with 4×4 transfer matrix, with added numerical complexity.

A.2 Calculation of the absorption of the superlattice

Optical absorption in a semiconductor material is one of the very important physical phenomena to be considered for the application in many optoelectronic devices. The parameter that characterizes the optical absorption is called the absorption coefficient and is defined as the ratio of the number of photons absorbed per unit volume per second to the number of photons injected per unit area per second. Hence the absorption coefficient gives the fraction of photons absorbed per unit distance and is denoted by α (cm^{-1}).

The absorption coefficient, α in the crystal for a bulk semiconductor is given as

$$\alpha(\hbar\omega) = 2A_0 \sum_n |\phi_n(0)|^2 \delta(\hbar\omega - E_g - E_n) \quad (A6)$$

where, $A_0 = \frac{\pi e^2 |\hat{i} \cdot \mathbf{p}_{cv}|^2}{n_r c \epsilon_0 m_0^2 \omega}$, \hat{i} is the unit vector along the direction of the propagation of the

incoming photon, \mathbf{p}_{cv} is the transition matrix element between the conduction and valence band, e is an electronic charge, n_r is refractive index, c is the velocity of the electromagnetic wave in vacuum, ϵ_0 is the permittivity of the vacuum, m_0 is the electron mass, ω is the angular frequency of the incoming electromagnetic wave, \hbar is the Planck's constant/ 2π , $R_y = \frac{1}{(4\pi\epsilon_s)^2} \frac{\mu_r e^4}{2\hbar^2}$,

$\alpha_0 = \frac{4\pi\epsilon\hbar^2}{e^2 \mu_r}$, μ_r is the reduced effective mass of holes and electrons and is given as,

$\frac{1}{\mu_r} = \frac{1}{m_e} + \frac{1}{m_h}$, $\epsilon_s = K\epsilon_0$, K is a dielectric constant, $\phi_n(0)$ is a normalized wave function for both

bound and continuum states and is given as

$$\phi_n(0)|_{bound} = \frac{1}{\pi\alpha_0^3 n^3} \quad (A7)$$

and

$$\phi_E(0)|_{continuum} = \frac{e^{\pi/\sqrt{E/R_y}}}{4\pi R_y \alpha_0^3 \sinh(\pi/\sqrt{E/R_y})}, \quad (A8)$$

respectively. With inclusion of this, the total absorption (also called *Elliott* formula) due to both bound and continuum states in bulk semiconductor can be given as

$$\alpha(\hbar\omega) = \frac{A_0}{2\pi^2 R_y \alpha_0^3} \left[4 \sum_{n=1}^{\infty} \frac{\Gamma/n^3}{(\Xi + 1/n^2) + \Gamma^2} + \frac{\pi e^{\pi/\sqrt{\Xi}}}{\sinh(\pi/\sqrt{\Xi})} \right], \quad (A9)$$

where $\Xi = \frac{\hbar\omega - E_g}{R_y}$, and Γ is *Lorentzian* width corresponding to the phonon broadening.

For the superlattice structure discussed in the section IV, we will use an anisotropic medium approach, in which the absorption coefficient of the bulk material is modified to take care of the anisotropy introduced by the presence of the superlattice periodicity. As discussed in the section IV, due to the penetration of the carrier wavefunction into the adjacent wells separated by thin barriers in a superlattice, the coupling between the two neighboring wells is very large to allow for the hybridization of the original discrete energy levels of isolated wells into minibands. The electron and hole tunneling through the minibands leads to the motion in the growth direction, which is characterized by the effective masses modified by the superlattice potential. Superlattice is then characterized by a three dimensional effective medium with different in-plane and growth-direction effective masses.

The superlattice absorption coefficient then can be assumed as a deviation from a bulk absorption coefficient by considering the anisotropy introduced in the reduced effective masses of the carriers in the plane of the layers (in-plane reduced effective mass, $\mu_{||}$) and perpendicular to the plane of layers (growth-direction or transverse reduced effective mass, μ_{\perp}), respectively. The ratio of these two masses can be defined as an anisotropy parameter,

$$\gamma = \mu_{||}/\mu_{\perp} \quad (A10)$$

This parameter modifies the absorption coefficient as suggested in Ref. 53, and is given as

$$\alpha(\hbar\omega, \gamma) = \frac{A_0}{2\pi^2 R_y'(\gamma) \alpha_0'(\gamma)^3} \left(\frac{2}{1+\gamma} \right)^2 \left[4 \sum_{n=1}^{\infty} \frac{\Gamma/n^3}{(\varepsilon'(\gamma) + 1/n^2) + \Gamma^2} + \frac{\pi e^{\pi/\sqrt{\Xi'(\gamma)}}}{\sinh(\pi/\sqrt{\Xi'(\gamma)})} \right] \quad (A11)$$

where

$$\Xi'(\gamma) = \frac{\hbar\omega - E_g}{R_Y'(\gamma)}, \quad \alpha_0'(\gamma) = \frac{4\pi\epsilon_s \hbar^2}{e^2 m_{\parallel}}, \quad R_Y'(\gamma) = \frac{1}{(4\pi\epsilon_s)^2} \frac{m_{\parallel} e^4}{2\hbar^2}, \quad m_{\parallel} = \frac{2\mu_{\parallel}}{1+\gamma}.$$

The in-plane and transverse reduced effective mass can be calculated as

$$\frac{1}{\mu_{\parallel}} = \frac{1}{m_{e\parallel}} + \frac{1}{m_{h\parallel}}, \quad \frac{1}{\mu_{\perp}} = \frac{1}{m_{e\perp}} + \frac{1}{m_{h\perp}} \quad (\text{A12})$$

The in-plane effective mass, m_{\parallel} is assumed to be average of effective masses of two different layers, w and b of thickness L_w and L_b respectively, in superlattice

$$m_{i\parallel} = \frac{m_i^w L_w + m_i^b L_b}{L_w + L_b} \quad \text{with } i=e, lh \text{ or } hh. \quad (\text{A13})$$

As a first approximation transverse effective mass, m_{\perp} can be obtain from

$$\frac{1}{m_{\perp}} = \frac{1}{\hbar^2} \left. \frac{d^2 E}{dq^2} \right|_{q=0} \quad (\text{A14})$$

where, energy E is extracted from a dispersion relation for a superlattice

$$\cos(qd) = \cos(k_w L_w) \cosh(k_b L_b) - \frac{1}{2} \left(\xi - \frac{1}{\xi} \right) \sinh(k_b L_b) \sin(k_w L_w) \quad (\text{A15})$$

here, $k_w = \sqrt{\frac{2m_w E}{\hbar^2}}$, $k_b = \sqrt{\frac{2m_b (V - E)}{\hbar^2}}$ for $E < V$ and $\xi = \frac{k_w m_b}{k_b m_w}$.

Using equations (15) and (16), we may derive the transverse effective mass as

$$\begin{aligned} m_{\perp} = & -\frac{\hbar^2}{d^2} \left[-\cos(L_w k_w) \sinh(L_b k_b) L_b B - \sin(L_w k_w) \cosh(L_b k_b) L_w A \right] \\ & -\frac{\hbar^2}{d^2} \left[-\frac{1}{2} \frac{1}{\xi^2} \frac{m_b}{m_w} \left(\frac{A}{k_b} + \frac{B k_w}{k_b^2} \right) \sinh(L_b k_b) \sin(L_w k_w) \right] \\ & -\frac{\hbar^2}{d^2} \left[-\frac{1}{2} \left\{ \xi - \frac{1}{\xi} \right\} \left\{ -\cosh(L_b k_b) \sin(L_w k_w) L_b B + \sinh(L_b k_b) \cos(L_w k_w) L_w A \right\} \right] \end{aligned} \quad (\text{A16})$$

where, $A = \sqrt{\frac{m_w}{2\hbar^2 E}}$, $B = \sqrt{\frac{m_b}{2\hbar^2 (V - E)}}$ and $d = L_w + L_b$.

Since the dielectric constant of GaAs(N) and AlGaAs are not very different from each other, the ratio of the in-plane and transverse dielectric constants for a superlattice structure is ~ 1 . Hence, the dielectric constant of the superlattice is taken as the weighted average for two layers of superlattice as

$$\varepsilon^2 = \frac{\varepsilon_w L_w + \varepsilon_b L_b}{L_w / \varepsilon_w + L_b / \varepsilon_b}. \quad (\text{A17})$$

For $\gamma=1$, equation (A11) becomes similar to the equation (A9) and the condition corresponds to the one of no-anisotropy or the bulk material absorption coefficient.

LIST OF ACRONYMS, ABBREVIATIONS, AND SYMBOLS

Acronym/ Abbreviation	Description
AM0	Air Mass Zero
BAC	Band Anti-Crossing
EOL	End of life
IBSC	Intermediate Band Solar cell
SL	Superlattice
SRH	Shockley Reed Hall

Symbol	Description
α	Absorption coefficient
E-	Lower branch of conduction band of dilute nitride
E+	Upper branch of the conduction band of dilute nitride
E _g	Bandgap
ϕ	Radiation flux
η	efficiency
L	Minority Carrier Diffusion length
KL	Radiation coefficient

DISTRIBUTION LIST

DTIC/OCF

8725 John J. Kingman Rd, Suite 0944

Ft Belvoir, VA 22060-6218

1 cy

AFRL/RVIL

Kirtland AFB, NM 87117-5776

2 cys

Official Record Copy

AFRL/RVSV/David Wilt

1 cy

(This page intentionally left blank)